Global Gene Expression Analysis of Cellular Death Mechanisms Induced by Mesoporous Silica Nanoparticle-Based Drug Delivery System

ARTICLE *in* ACS NANO · JANUARY 2014

Impact Factor: 12.88 · DOI: 10.1021/nn4046985 · Source: PubMed

3 AUTHORS, INCLUDING:

Qianjun He

69 PUBLICATIONS **3,264** CITATIONS

SEE PROFILE

Global Gene Expression Analysis of Cellular Death Mechanisms Induced by Mesoporous Silica Nanoparticle-Based Drug Delivery System

Xiaoyu Li, Qianjun He, and Jianlin Shi*

State Key Laboratory of High Performance Ceramics and Superfine Microstructure, Shanghai Institute of Ceramics, Chinese Academy of Sciences, 1295 Ding-Xi Road, Shanghai 200050, China

ABSTRACT Mesoporous silica nanoparticles (MSNs), as one of the most promising inorganic drug carriers, have attracted ever increasing attention due to their unique structural, physicochemical, and biochemical features. Drug delivery systems (DDSs) based on MSNs could easily escape from endosomes after endocytosis and protect the loaded drugs from bioerosion by stable MSN carriers, efficiently deliver drugs intracellularly in a sustained release way, and consequently kill cancer cells at enhanced efficacy. However, the underlying pathways and mechanisms of cancer cell death induced by MSN-mediated drug delivery have not been well explored. In this study, we introduce gene expression analyses to evaluate the pathways and mechanisms of cancer cell death induced by a MSN-based drug delivery system. Unique changes in gene expressions and gene ontology terms, which were caused only by the MSN-based DDS (DOX-loaded MSNs, DOX@MSNs) but not by free drug doxorubicin (DOX) and/or the carrier MSNs, were discovered and proposed to be responsible for the varied cell death mechanisms, including the greatly enhanced necrosis due to amplified oxidative stress and the apoptosis related with DNA/RNA synthesis and cell cycle inhibitions. By virtue of a certain kind of synergetic biological effect between the drug and the carrier, the DOX@MSNs DDS was found capable of increasing the intracellular levels of reactive oxygen species and triggering the mitochondria-related autophagic lysosome pathway, consequently activating a specific pathway of necrosis, which is different from those by the free drug and the carrier.

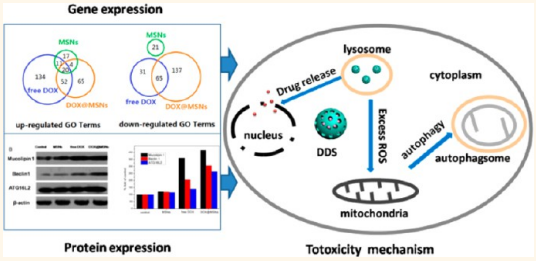

KEYWORDS: mesoporous silica nanoparticles · drug delivery · cytotoxicity · death mechanism · gene expression analysis

Nanomaterials are attracting ever-increasing attention in various fields, especially in biomedicines. Mesoporous silica nanoparticles (MSNs) as a kind of excellent inorganic carrier have aroused great interest due to their unique physicochemical and biochemical stability and a number of favorable structural features, such as uniform and tunable particles and pore size, high surface area and pore volume, facile surface functionalization, *etc.*[1−5] In the past decade, MSNs have been widely investigated as a drug carrier to construct drug delivery systems (DDSs) for targeted drug delivery and controlled drug release.[6−11] The biocompatibility of MSN carriers and the cytotoxicity of MSN-based DDSs have been extensively investigated;[12−17] however, the molecule-level interaction mechanisms between cells and drug molecules, MSN carriers or MSN-based DDSs, and the cell death pathways are not clear yet but are very important for the guidance of new drug design and application.

The drug efficacy of MSN-based DDSs, as compared to corresponding free drugs, has been widely reported to be significantly or even remarkably enhanced after incubations for reasonably long time periods, most probably resulting from the easy intracellular drug delivery and release.[18−22] In addition, several studies have also indicated that the integration of nanoparticles and drug molecules can generate synergistic effects, which leads to the increased sensitivity of cells to drugs by unique drug transferring and action pathways different from free drugs.[23,24] Large amounts of cytotoxicity data about MSN-based DDSs have been obtained, but the detailed death pathways

* Address correspondence to jlshi@mail.sic.ac.cn.

Received for review September 7, 2013 and accepted January 6, 2014.

Published online January 06, 2014
10.1021/nn4046985

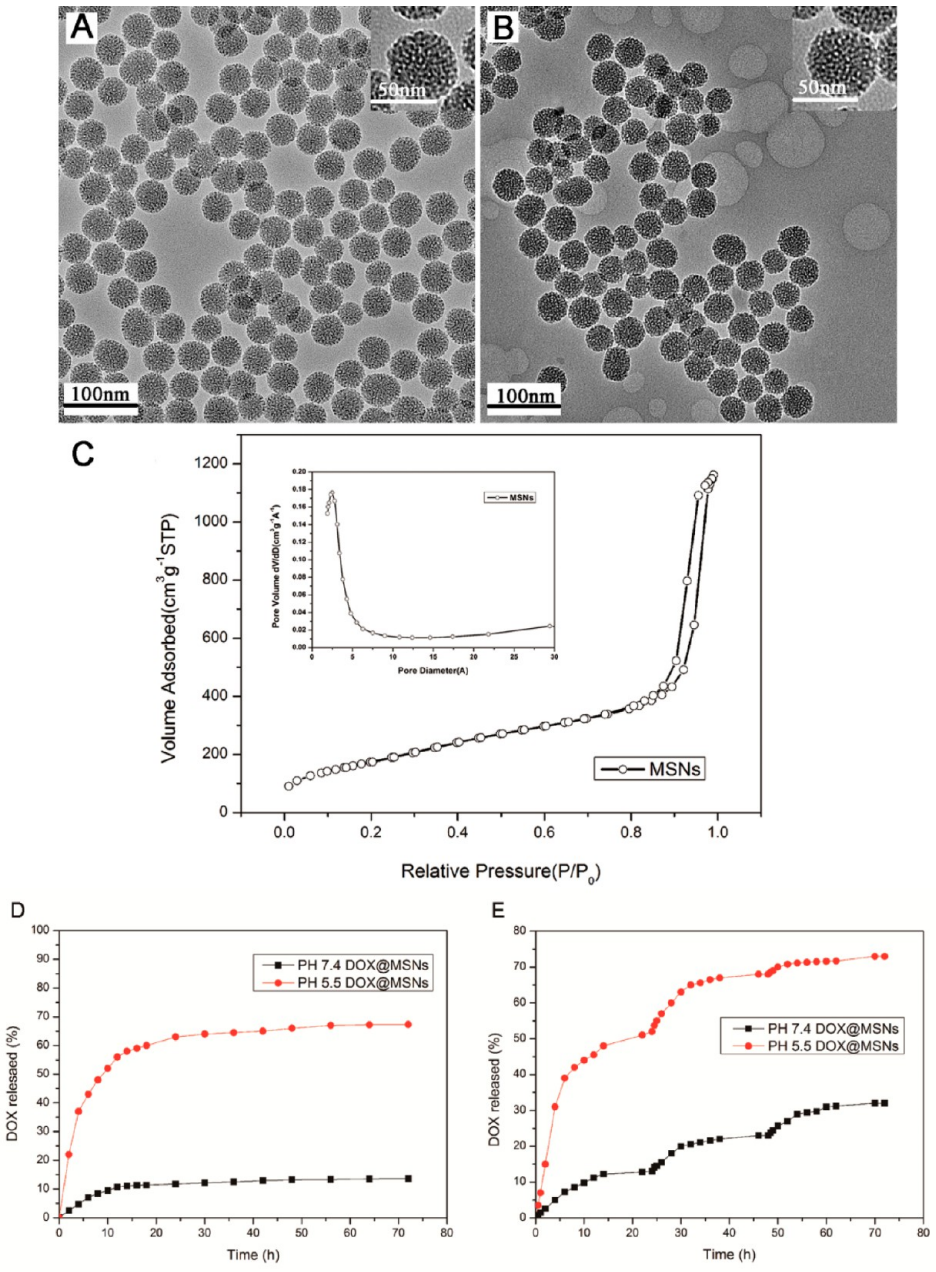

Figure 1. TEM images of MSNs (A) and DOX@MSNs (B), nitrogen adsorption−desorption isotherms and pore size distribution (the inset) of MSNs (C), DOX drug release profiles and accumulative release profiles (every 24 h the previous PBS was replaced by the fresh one) from DOX@MSNs in pH = 7.4 and pH = 5.5 PBS at 37 °C (D,E).

and mechanisms for MSN-based DDSs have not been reported yet.

Here, in the present study, we aim to find out the possible pathways and mechanisms of cell death induced by the DOX@MSNs DDS on the molecular level by employing a global gene expression analysis technology for the first time. DNA microarrays were used to investigate and compare the global gene expressions of cancer cells treated with a MSN carrier, free DOX drug, and the DOX@MSNs DDS and then clarify the cell death pathways and molecular mechanisms of drug efficacy enhancement by the DOX@MSNs DDS. Doxorubicin (DOX) was selected as a model drug because it is a broad-spectrum amphiphilic anticancer drug clinically used for the treatment of many types of cancers.[25] HeLa cells were selected as a kind of model cancer cells and used together with 4T1 cells and MCF-7 cells to perform significance of cytotoxicity. The gene expression changes induced by free DOX, MSNs, and DOX@MSNs were revealed by the gene ontology (GO) analysis.

RESULTS AND DISCUSSION

Characterization of MSNs. From TEM images (Figure 1A), the synthesized MSNs exhibit a very uniform particle size distribution around 40−50 nm, a regular spherical morphology, a clear porous structure (the inset), and a

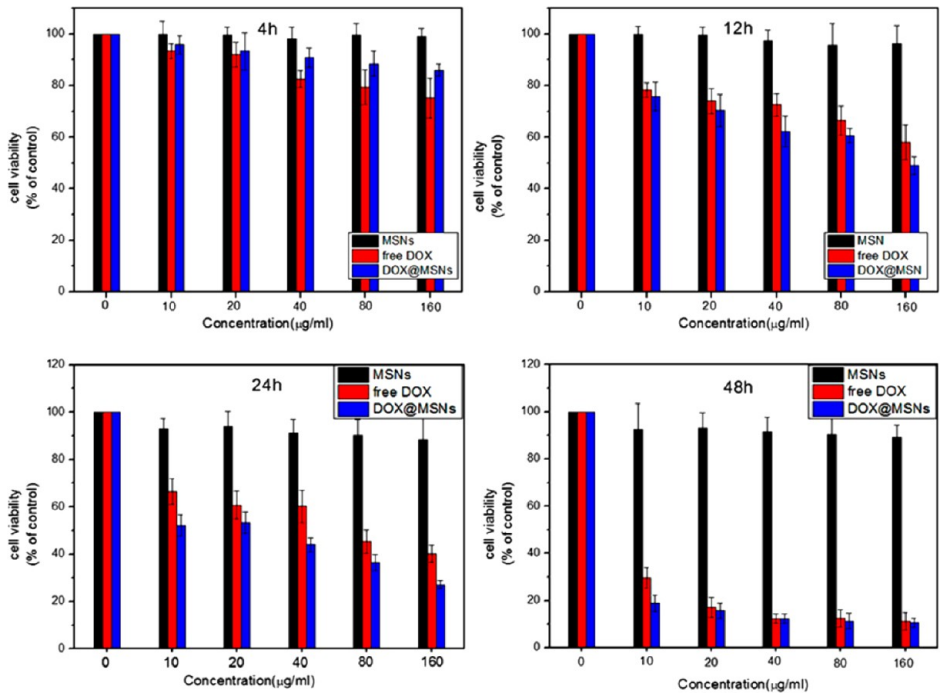

Figure 2. Cytotoxicity comparison among MSNs, free DOX, and DOX@MSNs against HeLa cells incubated for varied time durations.

perfect monodispersivity. BET measurement results (Figure 1C) indicate that MSNs have a high surface area of 721 cm^3/g and a narrow distribution of pore size centered at 2.3 nm (the inset) in accordance with the above TEM results. DOX was successfully loaded into MSNs with a drug loading capacity of 8 wt %, which was confirmed by UV−vis measurements at the wavelength of 488 nm. The morphology, size, and dispersivity of the DOX-loaded MSNs (DOX@MSNs) are almost the same as those of MSNs (Figure 1B), indicating no visible effect of the DOX loading on these aspects. Figure 1D,E, respectively, shows the drug release profiles in a constant release medium and in regularly replaced medium in an interval of 24 h of different pH values. A pH-responsive and sustained release behavior is clearly observed. No more than 13.6% of DOX releases from DOX@MSNs in the pH = 7.4 PBS (phosphate buffered saline) in 24 h, while about 65% of the release amount is achieved in the pH = 5.5 acidic PBS in 24 h (Figure 1D). Beyond 24 h, the drug releases reach a balance, resulting in the partial residual of the DOX payload (Figure 1D). However, it does not mean that the residual DOX could not be released.[26] When we exchanged the release media with fresh ones on an interval of 24 h, DOX can release again distinctly (Figure 1E). After 3 cycles of medium exchanging, the DOX-released amount reaches 73% (at pH = 5.5) in 72 h (Figure 1E), which is distinctly higher than the case without medium exchanging (about 65%, Figure 1D). Therefore, we think that the residual DOX can be released continually if the release medium could be replaced regularly.[26] Moreover, the pH-responsive release behavior of DOX@MSNs can be attributed to the electrostatic interaction and hydrogen bonding between positively charged DOX molecules and negatively charged mesopores.[27−29] Positively charged DOX is easily adsorbed onto the negatively charged surface, mainly the inner pore surface, of MSNs, and the −OH groups on MSN surface can form hydrogen bonds with −OH groups in DOX. So DOX@MSNs exhibit very slow release in neutral environment. When the pH value is lowered, the excess H+ in the solution will weaken the interaction between DOX and MSN by the competitive adsorption with the drug molecules on the MSN surfaces.[29−31] Such a pH-responsive drug release behavior is particularly beneficial to oncotherapy.[32,33]

Cytotoxicity of MSNs and DOX@MSNs. Next, the cytotoxicities of free DOX, MSNs, and DOX@MSNs at different concentrations and for different incubation time durations against HeLa cells were evaluated by the MTT assay. From Figure 2, it can be seen that MSNs exhibit no significant cytotoxic effect in up to 24 h, but both DOX@MSNs and free DOX show significant cytotoxicities, which become more significant at increased drug concentrations and/or incubation durations. There is no significant difference in cytotoxicities between DOX@MSNs and free DOX during the early incubation in 4 h with HeLa cells, after that, however, the cytotoxicity of DOX@MSNs remains higher than that of free DOX under the same conditions though only the partial DOX amount in DOX@MSNs has released. The cytotoxicity difference between free DOX and DOX@MSNs became accumulatively distinct in

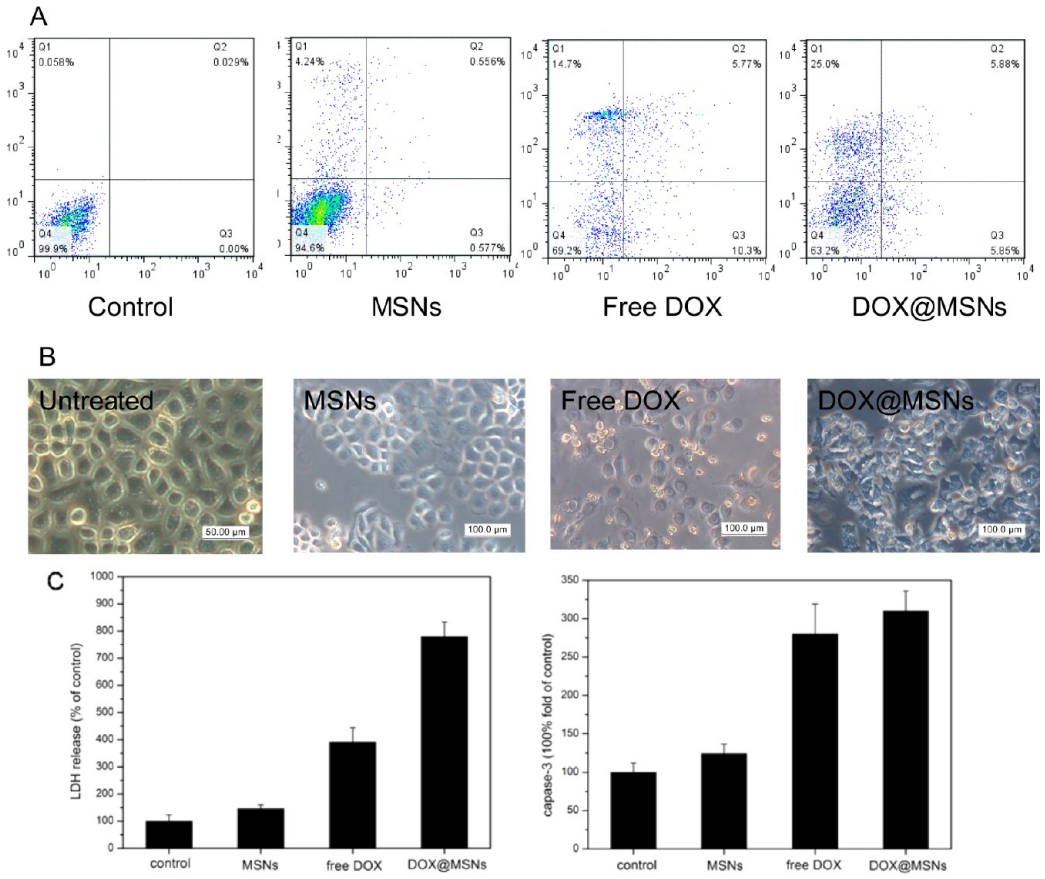

Figure 3. (A) Evaluation of the death pathways of HeLa cells treated with MSNs, free DOX, and DOX@MSNs at the equivalent DOX/MSNs concentration (80 μg/mL) for the same incubation time period (24 h). Q1, Q2, Q3, and Q4 zones represent necrosis, apoptosis, early apoptosis, and normality, respectively. (B) Optical images of HeLa cells. (C) Release of LDH and activity of capase-3 in cells treated with MSNs, free DOX, and DOX@MSNs; the value of control was set to 1.

24 h of incubation. Two other types of human breast cancer cells, 4T1 and MCF-7 cells, were also used to evaluate the cytotoxicities of MSNs, free DOX and DOX@MSNs by MTT assay. The results are similar with those treated HeLa cells (Figure S1 in Supporting Information), indicating that the cytotoxicity of DOX@MSNs is statistically significant among different cancer cells. Such an increasingly amplified cytotoxicity by drug delivery system DOX@MSNs was generally thought to result from the MSN-mediated endocytosis and the sustained intracellular release of DOX drug, as indicated by the *in vitro* release profile in Figure1D. The 48 h incubation leads to much decreased differences in cell viabilities especially at enhanced drug concentrations as most of the cells have been killed at the time.

Further, the death mechanisms of HeLa cells treated with the DOX@MSNs DDS and free drug DOX were evaluated and compared by flow cytometry (FCM) and fluorescence-activated cell sorting (FACS) approaches. As compared with blank control, MSNs exhibit very weak or negligible cytotoxicity against HeLa cells (Figure 3A), in accordance with the above-mentioned MTT assay. However, an apparent toxic effect of free DOX against HeLa cells could be visibly identified to be 14.7% of cellular necrosis, 5.77% of cellular apoptosis, and 10.3% of early apoptosis, suggesting that the cytotoxicity of free DOX is mainly related to the apoptosis-related cell death. By comparison, DOX@MSNs demonstrate a considerably enhanced fraction of cellular direct necrosis up to 25.0%, slightly enhanced cellular apoptosis to 5.88%, but much reduced early apoptosis down to 5.85%, indicating that the DOX@MSNs DDS not only maintains similar apoptosis effect of DOX but also significantly accelerates the direct necrosis effect of DOX against HeLa by a certain special action pathway. The cell necrosis in a very small percentage induced by MSNs by themselves could result from the enhanced reactive oxygen species (ROS) level (Figure 5).[34,35] The most important thing is that the necrosis is reinforced by the loading of DOX, while the pro-apoptotic power is partially lost. The partial loss in the pro-apoptotic power could be attributed to the very slow release of DOX from the carrier because of the sustained release behavior of DOX@MSNs (Figure 1D). Even so, the apoptosis can still be enhanced slightly (from 5.77 to 5.88%) while the necrosis is remarkably enhanced (from 14.7 to 25.0%). This apoptosis/necrosis-enhancing effect could result from the endocytosis-mediated intercellular drug delivery of DOX@MSNs, which is the different cellular

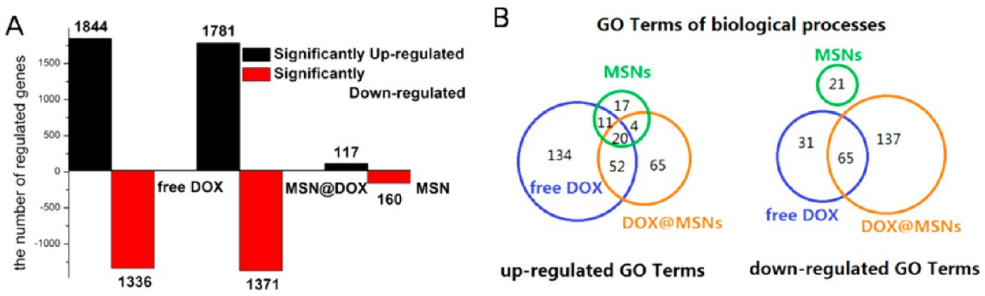

Figure 4. (A) Numbers of significantly changed genes in cells treated with free DOX, DOX@MSNs, and MSNs (equivalent DOX/MSNs concentration (80 μg/mL) for the same incubation time period of 24 h). (B) Numbers of significantly changed GO terms of biological process. Genes that demonstrated greater than log 2-fold change in the expression level were defined as significantly changed genes.

uptake route from that of free DOX (molecule diffusion route) and consequently causes the enhanced cytotoxicity. The mechanism demonstrates the advantage of the DOX@MSNs drug delivery system over free drug DOX. Furthermore, we have examined the levels of two key DAMP biomarkers, capase-3 and LDH release, to evaluate apoptosis and necrosis, respectively (Figure 3C).[36−39] The results indicate that the apoptosis (capase-3) is indeed enhanced slightly; meanwhile, the necrosis (LDH) is enhanced remarkably by the loading of DOX within MSNs, compared with free DOX, further confirming the FACS results (Figure 3A). Corresponding optical images also show significant difference between the cells treated with DOX@MSNs and free DOX: the morphology of HeLa cells treated with DOX@MSNs changes from spindle to irregular and cell size becomes bigger, while HeLa cells treated with free DOX overall shrink and become smaller, showing a typical apoptosis process.[40] Therefore, DOX@MSNs are thought to have a special mechanism for inducing cell death different from that of free DOX. However, both the detailed death pathways and the difference in the pathways between DOX@MSNs and free DOX remain unclear only by the simple cytotoxicity analysis.

Gene Expression Analysis. Hereinafter, we investigated the change in the global gene expressions of HeLa cells treated with DOX@MSNs and free DOX to find out the difference in their death pathways for the first time. As shown by Figure 4A, a total number of 3152 genes, including the 1781 up-regulated and the 1371 down-regulated, are significantly affected by DOX@MSNs and, correspondingly, a total of 3180 genes, including the 1844 up-regulated and 1336 down-regulated, by free DOX. Comparatively, the number of genes affected by MSNs was only approximately 1/10 of those by DOX-involved counterparts (total 297 genes with 117 up-regulated and 180 down-regulated). It can be seen that both DOX and DOX@MSNs have significantly disturbed the gene expression of HeLa cells; however, pure MSNs have only slightly. This should be the root causes leading to the difference in the cytotoxicity among them.

To distinguish the effects of MSNs, free DOX, and DOX@MSNs on the related biological processes of HeLa cells, the differentially up- and down-regulated gene levels were functionally classified on the basis of gene ontology. The up- and down-regulations of GO terms of biological processes affected by MSNs, free DOX, and DOX@MSNs are summarized and illustrated in Figure 4B. As shown in Figure 4B and Tables S6, S8, and S10 in Supporting Information, 217, 141, and 52 GO terms were significantly up-regulated by free DOX, DOX@MSNs, and MSNs, respectively (p value <0.001). Of these GO terms, there were 20 GO terms up-regulated in all three treatments (see Table S1 in Supporting Information), mainly referring to immune system process and cellular response to stress. Noticeably, DOX@MSNs lead to a more distinct immune system process than the others as the related p value of GO terms by DOX@MSNs is about 10^3 and 10^4 times lower than those by MSNs and free DOX, respectively. Comparatively, the response to stress is almost unaffected by DOX loading. Besides these 20 GO terms, additional 52 GO terms were also up-regulated jointly by DOX and DOX@MSNs (see Table S2 in Supporting Information), which are mainly related to the metabolic process, cell death and the regulation of apoptosis, and proliferation-related biological processes; however, DOX@MSNs show more significant effects than free DOX in up-regulating the gene expressions related with cell death such as apoptosis and proliferation-related biological processes. This indicates that the DOX@MSNs DDS does sensitize the DOX drug and intensify the apoptosis-induced toxic effect of DOX, though not very significant, even at the partial release of the DOX molecules, in accordance with the above death pathway analysis of HeLa cells. In addition to the common GO terms, the DOX@MSNs DDS individually up-regulated 65 GO terms, mainly referring to cell responses to oxidative stress generated by reactive oxygen species (ROS), and inorganic substance, *etc.* (see Figure 4B, Table 1, and Table S10 in Supporting Information). This indicates that DOX@MSNs uniquely activate the oxidative stress against HeLa cells, consequently causing cellular necrosis. Therefore, the

TABLE 1. Selected GO Terms of Biological Process Significantly Affected Only by DOX@MSNs (Complete Ones Can Be Found in Tables S6 and S7 in Supporting Information)

(a) up-regulated

GO.ID	term	count	*p* value
GO:0050776	regulation of immune response	135	1.55453×10^{-05}
GO:0010035	response to inorganic substance	96	1.81678×10^{-05}
GO:0009611	response to wounding	249	1.84703×10^{-05}
GO:0006979	response to oxidative stress	65	6.13472×10^{-05}
GO:0030155	regulation of cell adhesion	68	0.00014692
GO:0002684	positive regulation of immune system process	130	0.000153244
GO:0009991	response to extracellular stimulus	95	0.000174257
GO:0006916	antiapoptosis	73	0.000221447
GO:0000302	response to reactive oxygen species	36	0.000230239
GO:0034599	cellular response to oxidative stress	31	0.000330682
GO:0006643	membrane lipid metabolic process	36	0.000503061
GO:0042493	response to drug	85	0.000567028
GO:0034612	response to tumor necrosis factor	29	0.000758615
GO:0034976	response to endoplasmic reticulum stress	31	0.00076402

(b) down-regulated

GO.ID	term	count	*p* value
GO:0044260	cellular macromolecule metabolic process	1423	3.9639×10^{-37}
GO:0016070	RNA metabolic process	867	6.07779×10^{-23}
GO:0044237	cellular metabolic process	1700	1.36357×10^{-20}
GO:0044238	primary metabolic process	1699	6.8637×10^{-16}
GO:0051252	regulation of RNA metabolic process	674	2.88387×10^{-15}
GO:0019222	regulation of primary metabolic process	1020	3.13617×10^{-14}
GO:2001141	regulation of RNA biosynthetic process	653	6.18177×10^{-14}
GO:0032774	RNA biosynthetic process	689	3.2519×10^{-13}
GO:0008152	metabolic process	1804	8.23327×10^{-12}
GO:0044249	cellular biosynthetic process	987	3.867×10^{-09}
GO:0006281	DNA repair	113	7.77411×10^{-09}
GO:0006259	DNA metabolic process	208	2.87315×10^{-07}
GO:0006974	response to DNA damage stimulus	151	4.29592×10^{-07}
GO:0008380	RNA splicing	89	7.91035×10^{-06}
GO:0006260	DNA replication	75	2.28384×10^{-05}
GO:0016071	mRNA metabolic process	147	9.76518×10^{-05}
GO:0050684	regulation of mRNA processing	16	0.000344995
GO:0043484	regulation of RNA splicing	20	0.000771792

DOX@MSNs DDS has not only inherited and strengthened the apoptosis-induced cell death mechanism from DOX (DOX sensitization) but also triggered a unique and rather significant necrosis-induced cell death mechanism.

In the meantime, 96, 202, and 21 GO terms were significantly down-regulated in HeLa cells treated with free DOX, DOX@MSNs, and MSNs, respectively (Figure 4B and Table S5 in Supporting Information). It was found that the GO terms down-regulated by MSNs were completely different from those by DOX and DOX@MSNs but could be overlooked because the related *p* values were apparently much higher than those of DOX and DOX@MSNs (Tables S5 and S7). However, 65 GO terms were down-regulated jointly by DOX and DOX@MSNs (Figure 4B; see Table S5 in Supporting Information), which were mainly related with cell cycle (referring to nuclear division, M phase of mitotic cell cycle, *etc.*), organelle organization, and RNA processing. It was found that these significant terms were down-regulated much more by DOX@MSNs than by free DOX (Table S5), suggesting that the DOX@MSNs DDS can enhance the cell cycle blocking effect of DOX and suppress protein catabolic process and, therefore, induce more significant apoptosis *via* the DOX sensitization in accordance with the above death pathway analyses of HeLa cells of slightly enhanced apoptosis at only partial release of the drug. In addition to these common GO terms, the DOX@MSNs DDS individually down-regulated 137 GO terms remarkably, especially ones related to RNA biosynthetic process, RNA splicing, protein metabolic process, DNA repair, and cellular macromolecule metabolic process (Table 1b and Table S11 in Supporting Information). This implies that, in addition to sensitizing the independent effects of free DOX in the DOX@MSNs, the DOX@MSNs DDS also has an additional cell death mechanism *via*, for example, inhibiting the DNA repair, RNA splicing, and cellular macromolecule metabolic process of HeLa cells. It is noticeable that the levels of mainly down-regulated genes are far higher than those of up-regulated ones (Table 1).

Overall, cells treated with DOX@MSNs show a very different gene expression compared with those treated with free DOX and MSNs. DOX@MSNs induce the enhanced up-regulation level of apoptosis-related GO terms compared with free DOX *via* DOX sensitization, and more significantly, DOX@MSNs individually up-regulate GO terms related with oxidative stress, which are neither by free DOX nor by MSNs alone, indicating that the generation of ROS should be attributed to a certain kind of synergetic effect between them. Comparatively, DOX@MSNs also disturb GO terms related with RNA and DNA synthesis, splicing and metabolism, and regulations of many bioprocesses, which are not down-regulated by free DOX, nor by MSNs alone, also indicating a synergetic effect in killing the HeLa cells between them in the DOX@MSNs DDS *via* cell apoptosis.

So compared with free DOX, DOX@MSNs not only sensitize anticancer effect of DOX, even when DOX has only partially released, but also induce additional biological processes by the synergetic effects between the drug and the carrier, which caused promoted cell damages.

Effect of Intracellular ROS Generated by the DOX@MSNs DDS. Focusing on the above-mentioned necrosis-induced cell death mechanism mainly caused by oxidative stress, we further checked the intracellular levels of ROS in HeLa cells treated with free DOX, MSNs, and DOX@MSNs by DCFH-DA (2′,7′-dichlorodihydrofluorescein diacetate) staining method. As shown in Figure 5, it can be found that HeLa cells treated with MSNs exhibit relatively very weak green fluorescence; however, free DOX leads to considerable green

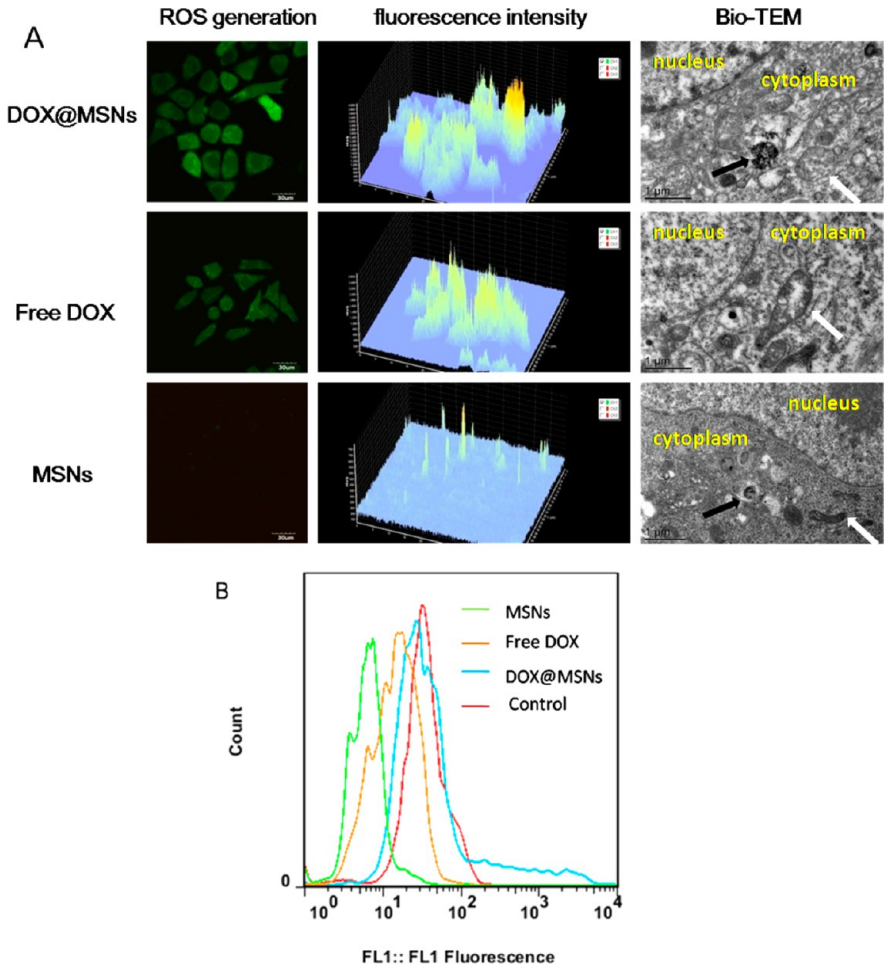

Figure 5. (A) Intracellular ROS levels and bio-TEM images of HeLa cells treated with DOX@MSNs, free DOX, and MSNs at the equivalent DOX/MSNs concentration (80 μg/mL) for the same incubation time period (24 h). The signal intensity maxima on vertical axis: 4000 (DOX@MSNs), 2600 (free DOX), and 750 (MSNs). In bio-TEM images, black arrows point the MSNs and white arrows point the mitochondria. (B) Quantification of ROS levels by FACS. The HeLa cells were incubated and dyed at the same condition with (A). Control represents positive control of ROS.

fluorescence and DOX@MSNs induce more intensive one, indicating that MSNs caused only a very low intracellular level of ROS in accordance with previous reports.[12,41,42] The DOX@MSNs DDS remarkably enhanced the intracellular ROS level compared with free DOX. Precise fluorescence quantification by FACS is given in Figure 5B, and the results are consistent with CLSM results, in which the fluorescence intensity representing the levels of ROS decreases from high to low in an order of DOX@MSNs, free DOX, and MSNs. Such an intracellular ROS-enhancing effect is thought to result from the intracellular delivery and sustained release of loaded drug DOX by/from MSNs and possibly a kind of unknown cooperative interaction between the drug DOX and the carrier MSNs. In a word, the oxidative stress against HeLa cells has been efficiently amplified by the DOX@MSNs DDS compared to free DOX, resulting in the up-regulation of the related GO terms as mentioned above.

ROS was previously found to be capable of inducing damages to mitochondria, consequently inducing the cellular necrosis.[12,43] Therefore, we investigated the effect of drugs on mitochondria of HeLa cells by electron microscopy. From Figure 5, MSNs can be found to have been wrapped in the vesicles in cytoplasm after incubation for 24 h with HeLa cells, and such an encapsulation of MSNs does not lead to visible damage to the cytoplasm structure and the mitochondria, which shows an almost unchanged regular shape and a complete and clear structure as compared to the blank control cells. Comparatively, mitochondria in HeLa cells treated with DOX@MSNs become largely swollen into an irregular morphology. In the meantime, as a comparison, cells treated with free DOX also exhibit an irregular and disintegrated inner structure of mitochondria but almost unchanged shape. The nucleoplasms of the cells treated with free DOX or the DDS are much less compact than that of the control, and nuclear membranes become indistinguishable. Mitochondria are organelles surrounded by a double membrane which are rich in polyunsaturated fatty acids (PUFA). The ROS such as OH^- radicals

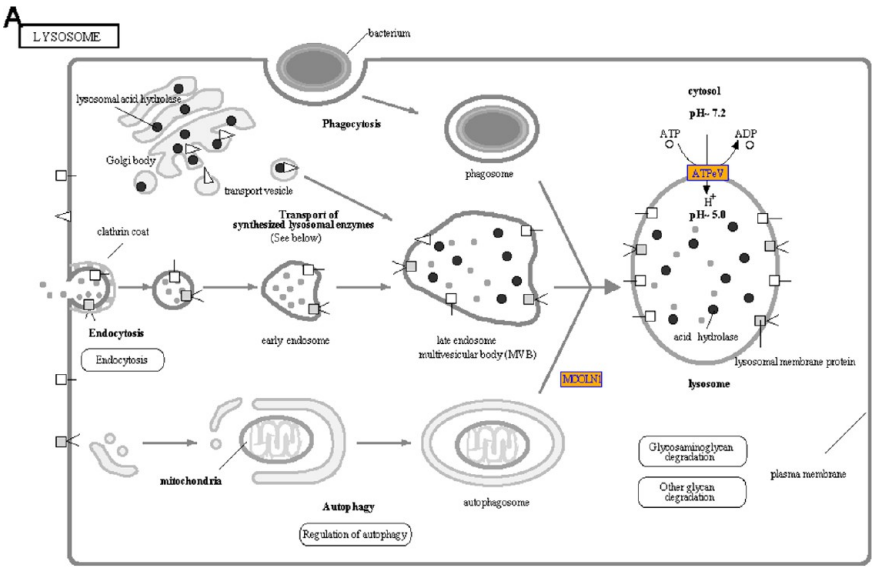

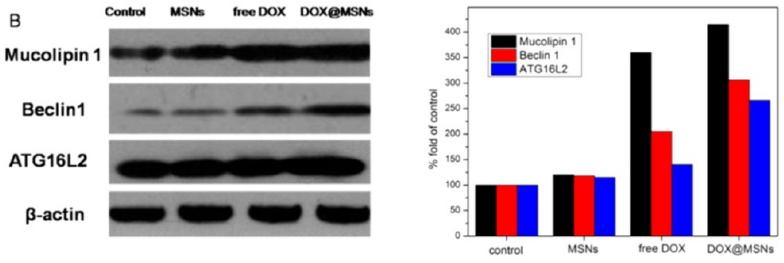

C

Genes	MSNs	Free DOX	DOX@MSNs
MCOLN1	nc	7.91	10.95
BECN1	nc	2.51	3.05
ATG16L2	nc	nc	2.96
ATG12	nc	3.1	4.24
ATG13	nc	4.90	5.13

Figure 6. (A) Most important part of lysosome KEGG pathways of HeLa cells up-regulated by DOX@MSNs. The orange and green represent up-regulated and unchanged gene expressions, respectively. Abbreviations for KEGG parameters can be found on the KEGG pathway webpage (http://www.genome.jp/kegg/pathway.html). (B) Western blotting analysis results of selected ATG-related proteins. The histogram (right) is the gray value of the three proteins against control; the value of control was set to 1. (C) Gene expression value of the related genes corresponding to the proteins evaluated in (B) (MCOLN1, BECN1, ATG16L1, and other ATG-related genes, ATG12 and ATG13). Nc represents no change.

can interact with PUFA, forming lipid peroxides and consequently enhancing the membrane permeability, causing swelling of mitochondria and other organelles.[44] So the bio-TEM results reveal that DOX@MSNs will bring about more mitochondrial damages and inhibit mitochondrial functioning through ROS.

KEGG Pathway Analysis. The KEGG (Kyoto Encyclopedia of Genes and Genomes) pathway mapping is a general analysis method to study cellular processes according to microarray gene spectra. Here the KEGG pathways are mapped by processing the global gene expression data to investigate the effect of the DOX@MSNs DDSs on cellular processes and reveal the potential cell death pathways. Among cellular processes, it can be found that the lysosome pathway is up-regulated by the DDS and partly up-regulated by free DOX (the most important part of lysosome pathway is shown in Figure 6A, and the whole pictures are shown in Figure S2). However, the pathway is neither up-regulated nor down-regulated by pure carrier MSNs, indicating that there is no significant effect of MSNs on cellular processes, in accordance with above-mentioned cytotoxicity results and GO terms' analyses.

From the up-regulated lysosome pathway, it can be found that the autophagic lysosome process is activated, in correspondence to the up-regulated MCOLN1, BECN1, and ATG-related genes, by both free DOX and DOX@MSNs (Figure 6A,C),[45,46] owing to the mitochondria damage induced by ROS generated from free/released DOX as mentioned above. To verify whether the gene-corresponding proteins have the same tendency of regulations with the genes, western blot analysis was used to measure the expressions of corresponding proteins, as shown in Figure 6B (left).

Mucolipin 1, Beclin 1 (BECN 1), and ATG16L2 as proteins related with autophagy were selected to correspond with genes MCOLN1, BECN 1, and ATG16L2 (ATGs, autophagy related genes) as also listed in Figure 6B (right).[47,48] It can be seen from the figure that these proteins share the similar tendency of regulations by MSNs, free DOX, and DOX@MSNs with the corresponding genes, which further confirms above results of the much enhanced gene regulations by the DOX@MSNs DDS compared with free DOX or MSN carrier.

The DOX@MSNs exhibit a stronger up-regulation effect on the lysosome process than free DOX, as suggested by much higher gene and protein enrichment values in Figure 6B, which indicates that DOX@MSNs lead to more significant damages to mitochondria of HeLa cells than free DOX. The above analysis on autophagic lysosome process is consistent with the significantly affected apoptosis-related GO terms, the misregulation of cell metabolism (Figure 4), and the much enhanced intracellular ROS level by DOX@MSNs DDS, which is also in accordance with above-mentioned bio-TEM analysis results (Figure 5).

Two following approaches are proposed for the highly activated lysosome pathway by DOX@MSNs DDS: (1) the phagocytosis of nanoparticles intensified the function of lysosome; (2) as above-mentioned, more serious organelle damage caused by apoptosis and other biological processes, as presented in Figure 4, induces excessive autophagy, which in return aggravates the cell death. In conclusion, DOX@MSNs can aggravate more cell death compared with free DOX.[49−51]

CONCLUSION

In this report, we first demonstrate that MSNs themselves can only induce very limited changes in gene expressions and therefore are generally a kind of biosafe drug deliverer without inducing undue cytotoxicity. Then the gene expression and gene ontology analyses of HeLa cells reveal that MSNs as a kind of drug (DOX) deliverer in DDSs are capable of significantly sensitizing DOX for killing the cancer cells as manifested by the intensified changes of common GO terms by the DDS in comparison with those by free DOX, more importantly, lead to the varied pathways of both necrosis and apoptosis in inducing the death of HeLa cancer cells from those by free DOX. The DOX@MSNs DDSs uniquely induce the up- and down-regulated GO terms which are not changed by either free DOX or MSNs individually, indicating the possible synergetic biological effects between the drug and the carrier in the DOX@MSNs DDS in killing the cancer cells. Especially, in addition to the pathways of DOX's killing HeLa cells *via* enhanced cell apoptosis by embedding in DNA and blocking the transcription and replication, DOX@MSNs can also induce the generation of a high level of ROS, thus damage the mitochondria, disturb cell cycle and many biological processes such as metabolism and synthesis, and finally enhance the cytotoxicity of the DDS to the cancer cells *via* necrosis. The present study reveals the underlying mechanisms of the enhanced cytotoxicity of MSN-mediated drug delivery on molecular levels *via* gene expression studies, which should be of great significance in the future development of highly efficient drug delivery systems for cancer chemotherapy, as well as the great needs for further investigations in understanding more detailed mechanisms of MSN-based DDS in cancer themotheray, such as the synergetic biological effect between the drug and the carrier.

MATERIALS AND METHODS

Materials. Tetraethyl orthosilicate (TEOS), triethanolamine (TEA), ethanol, methonal, hydrochloric acid (HCl, 37%), and sodium chloride (NaCl) were obtained from Sinopharm Chemical Reagent Co. Hexadecyl trimethylammonium chloride (CTAC, 25 wt %), 3-aminopropyltriethoxysilane (APTES), and rhodamine isothiocyanate (RITC) were obtained from Sigma-Aldrich. PBS solution (pH 7.4) was obtained from Shanghai Runcheng Biomedical Co., Ltd. Anticancer drug doxorubicin hydrochloride (DOX) was provided by Bejing HuaFeng United Technology Co., Ltd. Deionized water was used in all experiments. All chemicals were used as received without further purification.

Preparation of MSNs and DOX@MSNs. In order to get a high universality, MSNs of a normal size were necessary. Briefly, hexadecyl trimethylammonium chloride (2 g) and triethanolamine (0.02 g) were dissolved in turn in 20 mL of water under intensive stirring. Then the mixed solution was heated to 80 °C for 1 h, and 1.5 mL of tetraethyl orthosilicate was added dropwise with a continued stirring for another 1 h. The products were collected by centrifugation and washed three times with ethanol to remove the residual reactants. Next, the collected products were extracted for 3 h with a 1 wt % solution of sodium chloride in methanol at room temperature to remove the template CTAC. The step was repeated three times.

Five milligrams of MSNs was mixed with 5 mL of DOX solution in PBS (0.5 mg/mL). After being stirred for 24 h in the dark, the DOX-loaded particles were collected by centrifugation. To evaluate the DOX loading capacity, the supernatant solution was collected and the residual DOX contents were measured by UV−vis measurements at the wavelength of 488 nm. Calculation showed that the drug loading rate was 8%.

Nanoparticle Characterization. The morphology and mesostructure of nanoparticles were observed *via* transmission electron microscopy (TEM). TEM micrographs were obtained on a JEM-2010 electron microscope with an accelerating voltage of 200 kV. Dynamic light scattering (DLS) measurements were conducted on Zetasizer Nanoseries (Nano ZS90). Nitrogen adsorption−desorption isotherms at 77 K were measured on a Micrometitics Tristar 3000 system. All samples were pretreated for 4 h at 423 K under nitrogen before measurements. The pore size distribution was calculated from desorption branches of isotherms by the Barrett−Joyner−Halenda (BJH) method. Surface areas were calculated by the Brunauer−Emmett−Teller (BET) method.

***In Vitro* Drug Release.** Forty milligrams of the above-prepared DOX@MSNs in a 3500 Ka dialysis bag was immersed in 20 mL pH 7.4 PBS and pH 5.5 PBS at 37 °C and shaken at a speed of 100 rpm. At certain time intervals, 3 mL of the supernatant PBS was taken out to test the drug-released concentration by virtue of UV−vis absorption technique and then was returned to the original PBS. For accumulated release, PBS was replaced by fresh solution after every 24 h. The absorbances of the supernatant PBS at 488 nm were recorded on a Shimadzu UV-3101PC UV−vis absorption spectrophotometer.

Cell Culture. HeLa cells were seeded in culture dishes and plates with DMEM (GIBCO, New York) containing 10% fetal bovine serum (FBS, Sijiqing Biological Engineering Materials Co., Ltd., Hangzhou) at a concentration of 5000 cells/cm^2. After culturing in medium at 37 °C in a 5% CO_2 humidified environment for 48 h, the cell concentration reached 80%, ready for all the experiments. Then, the medium used to culture the cell plates was replaced with media containing MSNs, DOX@MSNs, and free DOX. Ninety-six-well culture plates were used for the MTT assay. Six-well culture plates were used for the FITC-PI staining, and 35 mm glass bottom dishes were used for confocal laser scanning microscopy (CLSM) imaging.

MTT Assay. HeLa cells were seeded at a concentration of 5000 cells/cm^2. After culturing for 48 h, MSNs, DOX@MSNs, and DOX were added to obtain a concentration of 10, 20, 40, 80, and 160 μg SiO_2/mL, and the cells were cultured for an additional 4/12/24/48 h. At the end of the incubation, the medium was removed, and 100 μL of MTT (3-(4,5-dimethylthiazol-2-yl)-2,5-diphenyltetrazolium bromide) solution (diluted in a culture media with a final concentration of 0.5 mg/mL) was added and incubated for another 4 h. Following incubation, the medium was removed and formazan crystals were solubilized by incubation for 15 min in 100 μL of dimethyl sulfoxide (DMSO). The absorbance of each well was read at a microplate reader (Bio-TekELx800) at the wavelength of 490 nm. The cytotoxicity was expressed as the percentage of cell viability compared to untreated control cells.

LDH Assay. Membrane leakage was quantified by detecting lactate dehydrogenase in the supernatant. LDH assay kit (Beyotime, China) was used. The absorbance was measured by a microplate reader (Bio-TekELx800) at the wavelength of 490 nm. Results are presented as relative values compared to control.

Capase-3 Activity Assay. The activity of caspase-3 was evaluated using the caspase-3 activity kit (Beyotime, China). The absorbance was measured by a microplate reader (Bio-TekELx800) at the wavelength of 405 nm. Results are presented as relative values compared to control.

Flow Cytometry Analysis. For cell death assay, flow cytometry was performed using an Annexin V-FITC apoptosis detection kit (Beyotime, China). After treatments with 80 μg of SiO_2/mL of MSNs and DOX@MSNs and the equivalent free DOX with the DOX in DOX@MSNs for 24 h, cells were detached by incubation with 0.25% trypsin for 5 min and centrifuged together with the primary medium at 1500*g* for 5 min, then washed by PBS twice. The cells were resuspended in 190 μL of binding buffer (10 mM), then 5 μL of Annexin V-FITC and 10 μL of propidium iodide (PI) were added and incubated for 15 min in the dark. Cells were assayed by flow cytometry, and data analysis was performed with Win MDI version 2.9.

Microarray Experiment. *RNA Labeling and Array Hybridization.* Cells cultured previously in DMEM for 48 h were further cultured for 24 h in media containing MSNs, DOX@MSNs, and DOX in DMEM (control). RNA quantity and quality were measured using NanoDrop ND-1000. RNA integrity was assessed using standard denaturing agarose gel electrophoresis.

Sample labeling and array hybridization were performed according to the Agilent one-color microarray-based gene expression analysis protocol (Agilent Technology). Briefly, total RNA from each sample was linearly amplified and labeled with Cy3-UTP. The labeled cRNAs were purified by RNeasy mini kit (Qiagen). The concentration and specific activity of the labeled cRNAs (pmol Cy3/μg cRNA) were measured by NanoDrop ND-1000. One microgram1 μg of each labeled cRNA was fragmented by adding 11 μL of 10× blocking agent and 2.2 μL of 25× fragmentation buffer, then heated at 60 °C for 30 min, and finally, 55 μL of 2× GE hybridization buffer was added to dilute the labeled cRNA. Then, 100 μL of hybridization solution was dispensed into the gasket slide and assembled to the gene expression microarray slide. The slides were incubated for 17 h at 65 °C in an Agilent hybridization oven. The hybridized arrays were washed, fixed and scanned with using the Agilent DNA Microarray Scanner (part number G2505C).

Microarray Data Analysis. *Data Analysis.* Agilent feature extraction software (version 11.0.1.1) was used to analyze the acquired array images. Quantile normalization and subsequent data processing were performed using the GeneSpring GX v11.5.1 software package (Agilent Technologies). After quantile normalization of the raw data, genes have flags in detected ("All Targets Value") were chosen for further data analysis. Differentially expressed genes were identified through fold change filtering. Hierarchical clustering was performed using the Agilent GeneSpring GX software (version 11.5.1). GO analysis and pathway analysis were performed in the standard enrichment computation method.

Measurement of Reactive Oxygen Species (ROS). For CLSM observations, HeLa cells were seeded at 5000 cells/cm^2 in coverglass bottom dishes. After culturing for 48 h, MSNs and DOX@MSNs were added with the same concentration of 80 μg SiO_2/mL and free DOX was added at the same concentration with the DOX in DOX@MSN. After the incubation for 24 h, the media were removed, and the cells were then washed twice with PBS solution to remove the residual nanoparticles.

Afterward, 2′,7′-dichlorodihydrofluorescein diacetate (DCFH-DA) (10 μM)/medium solution was added and incubated at 37 °C for 20 min to measure the generation of ROS. Then the cells were washed with PBS twice, and 1 mL of PBS was added and the cells were visualized under a confocal laser scanning microscope (FluoView FV1000, Olympus). The fluorescence images were taken under a 60× oil-immersion objective. Red and green luminescent emissions from DOX (RITC) and DCFH-DA were excited at the wavelength of 530 and 488 nm, respectively.

For FACS, cells were harvested and dyed as mentioned above. Cells were assayed by flow cytometry, and data analysis was performed with Win MDI version 2.9.

Bio-TEM Observation. The HeLa cells were incubated with 80 μg SiO_2/mL of MSNs and DOX@MSNs and the equivalent free DOX with the DOX in DOX@MSNs for 24 h. Then, the cells were washed with medium twice and detached by incubation with 0.25% trypsin for 5 min. The cells were harvested by centrifugation at 1500*g* for 5 min and fixed by glutaraldehyde at room temperature, then rinsed with PBS and dehydrated through a graded ethanol series, and finally cleared with propylene oxide. Then, the cell sample was embedded in EPOM812 and polymerized in an oven at 37 °C for 12 h, 45 °C for 12 h, and 60 °C for 48 h. Ultrathin sections of approximately 70 nm in thickness were cut with a diamond knife on a Leica UC6 ultramicrotome and transferred to the copper grid.

Western Blotting. For Western blotting, cells were harvested and washed and then were suspended in 100 mL of lysis buffer. Proteins were separated by 10% (w/v) SDS−polyacrylamide gel electrophoresis (SDS−PAGE) and then electrically transferred to a polyvinylidene difluoride membrane (Bio-Rad) after an equal amount of proteins was loaded in each lane. After blocking the membrane with 5% (w/v) skim milk, target proteins were immunodetected using specific antibodies. All primary antibodies for Western blotting were obtained from Cell Signaling Technology (Beverly, MA) and used at 1:1000 dilution. Thereafter, the horseradish peroxidase (HRP)-conjugated anti-rabbit IgG (Invitrogen) was applied as the secondary antibody, and the positive bands were detected using the Amersham ECL Plus Western blotting detection reagents (GE Health care, Piscataway, NJ).

Conflict of Interest: The authors declare no competing financial interest.

Acknowledgment. This work was financially supported by the National Natural Science Foundation of China (Grants 51132009, 51102259, 50823007, and 50972154), the Science

and Technology Commission of Shanghai (Grants 10430712800, 11nm0505000, and 11nm0506500).

Supporting Information Available: Cytotoxicity comparison of MSNs, free DOX, and DOX@MSNs against 4T1 cells and MCF-7 cells incubated for varied time durations are in Figure S1. The whole lysosome KEGG pathways of HeLa cells up-regulated by DOX@MSNs and free DOX are shown in Figure S2. The up-regulated and down-regulated GO terms affected by DOX@MSNs, free DOX, and MSNs in HeLa cells are listed in Tables S1−S11. This material is available free of charge *via* the Internet at http://pubs.acs.org.

REFERENCES AND NOTES

1. Zhang, Z. J.; Wang, L. M.; Wang, J.; Jiang, X. M.; Li, X. H.; Hu, Z. J.; Ji, Y. H.; Wu, X. C.; Chen, C. Y. Mesoporous Silica-Coated Gold Nanorods as a Light-Mediated Multifunctional Theranostic Platform for Cancer Treatment. *Adv. Mater.* **2012**, *24*, 1418–1423.
2. He, Q.; Shi, J.; Chen, F.; Zhu, M.; Zhang, L. An Anticancer Drug Delivery System Based on Surfactant-Templated Mesoporous Silica Nanoparticles. *Biomaterials* **2010**, *31*, 3335–3346.
3. Xie, M.; Shi, H.; Ma, K.; Shen, H.; Li, B.; Shen, S.; Wang, X.; Jin, Y. Hybrid Nanoparticles for Drug Delivery and Bioimaging: Mesoporous Silica Nanoparticles Functionalized with Carboxyl Groups and a Near-Infrared Fluorescent Dye. *J. Colloid Interface Sci.* **2013**, *395*, 306–314.
4. Li, W.; Zhao, D. Extension of the Stöber Method To Construct Mesoporous SiO_2 and TiO_2 Shells for Uniform Multifunctional Core−Shell Structures. *Adv. Mater.* **2013**, *25*, 142–149.
5. He, Q.; Shi, J. Mesoporous Silica Nanoparticle Based Nano Drug Delivery Systems: Synthesis, Controlled Drug Release and Delivery, Pharmacokinetics and Biocompatibility. *J. Mater. Chem.* **2011**, *21*, 5845–5855.
6. Chen, Y.; Chen, H. R.; Zhang, S. J.; Chen, F.; Zhang, L. X.; Zhang, J. M.; Zhu, M.; Wu, H. X.; Guo, L. M.; Feng, J. W.; *et al.* Multifunctional Mesoporous Nanoellipsoids for Biological Bimodal Imaging and Magnetically Targeted Delivery of Anticancer Drugs. *Adv. Funct. Mater.* **2011**, *21*, 270–278.
7. Tang, F.; Li, L.; Chen, D. Mesoporous Silica Nanoparticles: Synthesis, Biocompatibility and Drug Delivery. *Adv. Mater.* **2012**, *24*, 1504–1534.
8. Chen, F.; Zhu, Y. Chitosan Enclosed Mesoporous Silica Nanoparticles as Drug Nano-Carriers: Sensitive Response to the Narrow pH Range. *Microporous Mesoporous Mater.* **2012**, *150*, 83–89.
9. Lee, J. E.; Lee, N.; Kim, T.; Kim, J.; Hyeon, T. Multifunctional Mesoporous Silica Nanocomposite Nanoparticles for Theranostic Applications. *Acc. Chem. Res.* **2011**, *44*, 893–902.
10. Chen, Y.; Chen, H. R.; Zeng, D. P.; Tian, Y. B.; Chen, F.; Feng, J. W.; Shi, J. L. Core/Shell Structured Hollow Mesoporous Nanocapsules: A Potential Platform for Simultaneous Cell Imaging and Anticancer Drug Delivery. *ACS Nano* **2010**, *4*, 6001–6013.
11. Wang, X.; Chen, H. R.; Zheng, Y. Y.; Ma, M.; Chen, Y.; Zhang, K.; Zeng, D. P.; Shi, J. L. Au-Nanoparticle Coated Mesoporous Silica Nanocapsule-Based Multifunctional Platform for Ultrasound Mediated Imaging, Cytoclasis and Tumor Ablation. *Biomaterials* **2013**, *34*, 2057–2068.
12. Shim, W.; Paik, M. J.; Nguyen, D.-T.; Lee, J.-K.; Lee, Y.; Kim, J.-H.; Shin, E.-H.; Kang, J. S.; Jung, H.-S.; Choi, S. Analysis of Changes in Gene Expression and Metabolic Profiles Induced by Silica-Coated Magnetic Nanoparticles. *ACS Nano* **2012**, *6*, 7665–7680.
13. Di Pasqua, A. J.; Sharma, K. K.; Shi, Y.-L.; Toms, B. B.; Ouellette, W.; Dabrowiak, J. C.; Asefa, T. Cytotoxicity of Mesoporous Silica Nanomaterials. *J. Inorg. Biochem.* **2008**, *102*, 1416–1423.
14. Kim, J.-H.; Park, H. O.; Jang, S.-W.; Shin, C.-G.; Ryu, J.-C.; Kim, Y.-J.; Yang, S. I. Gene Expression Profiling Associated with Treatment of Positive Charged Colloidal Silica Nanoparticle in Human Neuroblastoma Cells. *BioChip. J.* **2011**, *5*, 317–326.
15. Guo, W. S.; Luo, Y.; Wei, K.; Gao, X. A Cellular Level Biocompatibility and Biosafety Evaluation of Mesoporous SiO_2-Based Nanocomposite with Lanthanum Species. *J. Mater. Sci.* **2012**, *47*, 1514–1521.
16. He, Q. J.; Zhang, Z. W.; Gao, F.; Li, Y. P.; Shi, J. L. *In Vivo* Biodistribution and Urinary Excretion of Mesoporous Silica Nanoparticles: Effects of Particle Size and PEGylation. *Small* **2011**, *7*, 271–280.
17. Yu, T.; Malugin, A.; Ghandehari, H. Impact of Silica Nanoparticle Design on Cellular Toxicity and Hemolytic Activity. *ACS Nano* **2011**, *5*, 5717–5728.
18. Gao, Y.; Yang, C.; Liu, X.; Ma, R.; Kong, D.; Shi, L. A Multifunctional Nanocarrier Based on Nanogated Mesoporous Silica for Enhanced Tumor-Specific Uptake and Intracellular Delivery. *Macromol. Biosci.* **2012**, *12*, 251–259.
19. Li, L. L.; Yin, Q.; Cheng, J.; Lu, Y. Polyvalent Mesoporous Silica Nanoparticle-Aptamer Bioconjugates Target Breast Cancer Cells. *Adv. Healthcare Mater* **2012**, *1*, 567–572.
20. Lee, J. E.; Lee, N.; Kim, H.; Kim, J.; Choi, S. H.; Kim, J. H.; Kim, T.; Song, I. C.; Park, S. P.; Moon, W. K. Uniform Mesoporous Dye-Doped Silica Nanoparticles Decorated with Multiple Magnetite Nanocrystals for Simultaneous Enhanced Magnetic Resonance Imaging, Fluorescence Imaging, and Drug Delivery. *J. Am. Chem. Soc.* **2009**, *132*, 552–557.
21. Zhao, Y.; Lin, L. N.; Lu, Y.; Chen, S. F.; Dong, L.; Yu, S. H. Templating Synthesis of Preloaded Doxorubicin in Hollow Mesoporous Silica Nanospheres for Biomedical Applications. *Adv. Mater.* **2010**, *22*, 5255–5259.
22. Yuan, L.; Tang, Q.; Yang, D.; Zhang, J. Z.; Zhang, F.; Hu, J. Preparation of pH-Responsive Mesoporous Silica Nanoparticles and Their Application in Controlled Drug Delivery. *J. Phys. Chem. C* **2011**, *115*, 9926–9932.
23. Tao, Z. M.; Toms, B.; Goodisman, J.; Asefa, T. Mesoporous Silica Microparticles Enhance the Cytotoxicity of Anticancer Platinum Drugs. *ACS Nano* **2010**, *4*, 789–794.
24. Barraud, L.; Merle, P.; Soma, E.; Lefrançois, L.; Guerret, S.; Chevallier, M.; Dubernet, C.; Couvreur, P.; Trépo, C.; Vitvitski, L. Increase of Doxorubicin Sensitivity by Doxorubicin-Loading into Nanoparticles for Hepatocellular Carcinoma Cells *in Vitro* and *in Vivo*. *J.Hepato.* **2005**, *42*, 736–743.
25. Lebold, T.; Jung, C.; Michaelis, J.; Bräuchle, C. Nanostructured Silica Materials as Drug-Delivery Systems for Doxorubicin: Single Molecule and Cellular Studies. *Nano Lett.* **2009**, *9*, 2877–2883.
26. He, Q.; Zhang, J.; Chen, F.; Guo, L.; Zhu, Z.; Shi, J. An Anti-ROS/Hepatic Fibrosis Drug Delivery System Based on Salvianolic Acid B Loaded Mesoporous Silica Nanoparticles. *Biomaterials* **2010**, *31*, 7785–7796.
27. Meng, H.; Liong, M.; Xia, T. Engineered Design of Mesoporous Silica Nanoparticles To Deliver Doxorubicin and P-Glycoprotein siRNA To Overcome Drug Resistance in a Cancer Cell Line. *ACS Nano* **2010**, *4*, 4539–4550.
28. Gao, Y.; Chen, Y.; Ji, X. Controlled Intracellular Release of Doxorubicin in Multidrug-Resistant Cancer Cells by Tuning the Shell-Pore Sizes of Mesoporous Silica Nanoparticles. *ACS Nano* **2011**, *4*, 9788–9798.
29. Chen, Y.; Chen, H.; Zhang, S. Structure-Property Relationships in Manganese Oxide-Mesoporous Silica Nanoparticles Used for T_1-Weighted MRI and Simultaneous Anti-cancer Drug Delivery. *Biomaterials* **2012**, *33*, 2388–2398.
30. Lee, E. S.; Gao, Z. G.; Bae, Y. H. Recent Progress in Tumor pH Targeting Nanotechnology. *J. Controlled Release* **2008**, *132*, 164–70.
31. Gao, C.; Zheng, H.; Xing, L. Designable Coordination Bonding in Mesopores as a pH-Responsive *Release System*. *Chem. Mater.* **2010**, *22*, 5437–5444.
32. Du, J. Z.; Sun, T. M.; Song, W. J.; Wu, J.; Wang, J. A. Tumor-Acidity-Activated Charge-Conversional Nanogel as an Intelligent Vehicle for Promoted Tumoral-Cell Uptake and Drug Delivery. *Angew. Chem., Int. Ed.* **2010**, *49*, 3621.
33. Ganta, S.; Devalapally, H.; Shahiwala, A.; Amiji, M. A Review of Stimuli-Responsive Nanocarriers for Drug and Gene Delivery. *J. Controlled Release* **2008**, *126*, 187–204.

34. Mailloux, A.; Grenet, K.; Bruneel, A. Anticancer Drugs Induce Necrosis of Human Endothelial Cells Involving Both Oncosis and Apoptosis. *Eur. J. Cell. Biol.* **2001**, *80*, 442–449.
35. Bauer, A. T.; Strozyk, E. A.; Gorzelanny, C. Cytotoxicity of Silica Nanoparticles through Exocytosis of Von Willebrand Factor and Necrotic Cell Death in Primary Human Endothelial Cells. *Biomaterials* **2011**, *32*, 8385–8393.
36. Liu, Y.; Zhang, S. P.; Ca, Y. Q. Cytoprotective Effects of Selenium on Cadmium-Induced LLC-PK1 Cells Apoptosis by Activating JNK Pathway. *Toxicol. in Vitro* **2007**, *21*, 677–684.
37. Liu, C.; Yu, K.; Shi, X. Induction of Oxidative Stress and Apoptosis by PFOS and PFOA in Primary Cultured Hepatocytes of Freshwater Tilapia (*Oreochromis niloticus*). *Aquat. Toxicol.* **2007**, *82*, 135–143.
38. Chang, J. S.; Chang, K. L. B.; Hwang, D. F. *In Vitro* Cytotoxicitiy of Silica Nanoparticles at High Concentrations Strongly Depends on the Metabolic Activity Type of the Cell Line. *Environ. Sci. Technol.* **2007**, *41*, 2064–2068.
39. Kim, T. H.; Kim, M.; Park, H. S. Size-Dependent Cellular Toxicity of Silver Nanoparticles. *J. Biomed. Mater. Res. A* **2012**, *100*, 1033–1043.
40. Kerr, J. F.; Wyllie, A. H.; Currie, A. R. Apoptosis: A Basic Biological Phenomenon with Wide-Ranging Implications in Tissue Kinetics. *Brit. J. Cancer* **1972**, *26*, 239.
41. Park, E.-J.; Park, K. Oxidative Stress and Pro-inflammatory Responses Induced by Silica Nanoparticles *in Vivo* and *in Vitro*. *Toxicol. Lett.* **2009**, *184*, 18–25.
42. Wang, F.; Jiao, C.; Liu, J.; Yuan, H.; Lan, M.; Gao, F. Oxidative Mechanisms Contribute to Nanosize Silican Dioxide-Induced Developmental Neurotoxicity in PC12 Cells. *Toxicol. in Vitro* **2011**, *25*, 1548–1556.
43. Xu, J.; Xu, P.; Li, Z.; Huang, J.; Yang, Z. Oxidative Stress and Apoptosis Induced by Hydroxyapatite Nanoparticles in C6 Cells. *J. Biomed. Mater. Res. A* **2012**, *100*, 738–745.
44. Antunes, F.; Cadenas, E.; Brunk, U. Apoptosis Induced by Exposure to a Low Steady-State Concentration of H_2O_2 Is a Consequence of Lysosomal Rupture. *Biochem. J.* **2001**, *356*, 549–555.
45. Fukui, M.; Kang, K. S.; Okada, K.; Zhu, B. T. EPA, an Omega-3 Fatty Acid, Induces Apoptosis in Human Pancreatic Cancer Cells: Role of ROS Accumulation, Caspase-8 Activation, and Autophagy Induction. *J. Cell. Biochem.* **2013**, *114*, 192–203.
46. Kondo, Y.; Kondo, S. Autophagy and Cancer Therapy. *Autophagy* **2006**, *2*, 85–90.
47. Liang, X. H.; Jackson, S.; Seaman, M. Induction of Autophagy and Inhibition of Tumorigenesis by Beclin 1. *Nature* **1999**, *402*, 672–676.
48. Cremer, T. J.; Amer, A. O.; Tridandapani, S. *Francisella tularensis* Regulates Autophagy-Related Host Cell Signaling Pathways. *Autophagy* **2009**, *5*, 125–128.
49. Simonsen, A.; Cumming, R. C.; Brech, A. Promoting Basal Levels of Autophagy in the Nervous System Enhances Longevity and Oxidant Resistance in Adult Drosophila. *Autophagy* **2008**, *4*, 176–184.
50. Chen, Y.; McMillan-Ward, E.; Kong, J. Oxidative Stress Induces Autophagic Cell Death Independent of Apoptosis in Transformed and Cancer Cells. *Cell Death Differ.* **2008**, *15*, 171–182.
51. Gozuacik, D.; Kimchi, A. Autophagy as a Cell Death and Tumor Suppressor Mechanism. *Oncogene* **2004**, *23*, 2891–2906.